OPEN ACCESS
Journal of Innovative Optical Health Sciences
Vol. 17, No. 1 (2024) 2350011 (8 pages)

DOI: 10.1142/S1793545823500116

World Scientific
www.worldscientific.com

In vivo label-free measurement of blood flow velocity symmetry based on dual line scanning third-harmonic generation microscopy excited at the 1700 nm window

Hui Cheng, Jincheng Zhong, Ping Qiu*,‡ and Ke Wang†,‡
Key Laboratory of Optoelectronic Devices
and Systems of Ministry of Education and Guangdong Province
College of Physics and Optoelectronic Engineering
Shenzhen University, Shenzhen 518060 P. R. China
*pingqiu@szu.edu.cn
†kewangfs@szu.edu.cn

Received 10 March 2023
Accepted 11 April 2023
Published 20 May 2023

Measurement of blood flow velocity is key to understanding physiology and pathology *in vivo*. While most measurements are performed at the middle of the blood vessel, little research has been done on characterizing the instantaneous blood flow velocity distribution. This is mainly due to the lack of measurement technology with high spatial and temporal resolution. Here, we tackle this problem with our recently developed dual-wavelength line-scan third-harmonic generation (THG) imaging technology. Simultaneous acquisition of dual-wavelength THG line-scanning signals enables measurement of blood flow velocities at two radially symmetric positions in both venules and arterioles in mouse brain *in vivo*. Our results clearly show that the instantaneous blood flow velocity is not symmetric under general conditions.

Keywords: 1700 nm-Window; third-harmonic generation imaging; blood flow velocity.

1. Introduction

For animals and human beings, blood vessels are critical for the circulation and efficient transport of nutrients, fluids, and signaling molecules between cellular tissues and organs.[1,2] Abnormal vascular development may contribute to the pathogenesis of many diseases, such as excessive angiogenesis, abnormal remodeling, and insufficiency or regression of vascular growth.[3–5] It has long been recognized that hemodynamics plays a decisive role in shaping blood vessels and mediating vascular disease. Brain is the one of most important organs and relies almost entirely on blood for the delivery of essential nutrients and energy. Besides, blood

‡Corresponding authors.

flow velocity in the cerebral vasculature can quantitatively reflect the physiological and pathological conditions, such as dynamic activity of nerve cells, cerebrovascular embolism, and peripheral blood flow abnormalities due to Alzheimer's disease.[6–8] Therefore, the blood flow velocity is an important parameter of the blood supply to the brain.

Besides the blood flow velocity itself, an interesting and unanswered question is: Is the blood flow velocity symmetric in brain blood vessels? Theoretically, for simplicity, it is often assumed that blood vessels are cylinders with radially symmetric velocity distribution.[9,10] However, this assumption is apparently not valid from a practical point of view. The measurement of the intravascular distribution of blood flow velocity is essential for answering this question and may be of significance for the study of cerebrovascular development, physiology and pathology. Many methods have been proposed to measure the blood flow velocity *in vivo*. Intrinsic optical imaging and laser scatter imaging can yield information about changes in oxygenation and/or blood flow, but are not suitable for high-resolution measurements of flow below the cortical surface.[11–14] Laser doppler imaging and blood oxygenation level-dependent functional magnetic resonance imaging (BLOD fMRI) measure deep into the brain surface but with lower temporal and spatial resolution.[15–17] Though single-photon imaging using confocal laser scanning microscopy is feasible for blood flow analysis at the single-vessel level, it has relatively poor spatial resolution in the z direction (along the light path) and its imaging depth is limited.[18–20] Moreover, for studies of vascular structure and blood flow, fluorescent dyes or beads are typically injected into the bloodstream to label the blood plasma.[21–24] However, the flow of fluorescent beads through the field of view is random, as is the position of measurement. In other words, this technology cannot measure instantaneous values at a designated position. Besides, these methods can only measure velocity at one position, and the blood flow velocity at different radial positions cannot be measured simultaneously, so, the above problem cannot be solved.

Multiphoton microscopy (MPM) is well known for its 3D sectioning capability, which enables locating to the equatorial plane of the blood vessel for velocity measurement. Third-harmonic generation (THG) is one of the frequent imaging modalities of MPM.[25–29] Red blood cells (RBCs) can produce THG signal under excitation at the appropriate wavelength.[30,31] Compared with other methods, THG imaging combines the advantages of a label-free technology with sub-micron spatial resolution and intrinsic 3D sectioning capability. Besides, excited at the 1700 nm window, it is an ideal method for continuously measuring blood flow velocity *in vivo*. Recently, we have demonstrated that THG imaging excited at the 1700 nm window can be applied to measuring blood flow velocity and even wall shear rate (i.e., velocity gradient) in animal models *in vivo*.[30,32]

In order to answer the key question of brain blood flow symmetry, here, we use a recently developed dual-wavelength label-free THG line-scanning technology[32] to measure the flow velocity at symmetric positions along both venules and arterioles in mouse brains *in vivo*. Using this technique, we can simultaneously extract the THG line-scanning traces at two radially symmetric positions within the vessel to calculate the flow velocities. Our results show the general asymmetric distribution of blood flow velocity at high spatial and temporal resolution in practical conditions which cannot be accounted for by the simple theoretical assumption of symmetry.

2. Materials and Methods

2.1. *Dual-wavelength third-harmonic-generation imaging system*

In order to obtain the blood flow velocity at two radially symmetric positions simultaneously, we use the dual-wavelength third-harmonic-generation line-scanning imaging system.[32] The experimental step is shown in Fig. 1(a). We used a half-wave plate to adjust the polarization angle of the 1550 nm, 6.25 MHz, and 527 fs pump laser (FLCPA-02CSZU, Calmar) output into a 3 m LMA fiber (LMA-PM-35, NKT Photonics). The soliton self-frequency shift (SSFS) effect in the fiber yielded two orthogonally-polarized laser pulses with two wavelengths simultaneously. Then, a customized 1650 nm long-pass filter (1650lpf, Yi Zhao Photonics Technology) was used to remove the residual pump at the output end of the fiber. After separating these two wavelengths (1680 nm and 1780 nm) spatially using a polarization beam splitter (PBS104, Thorlabs), the measured spectra of these two solitons are shown in Fig. 1(b). The pulse

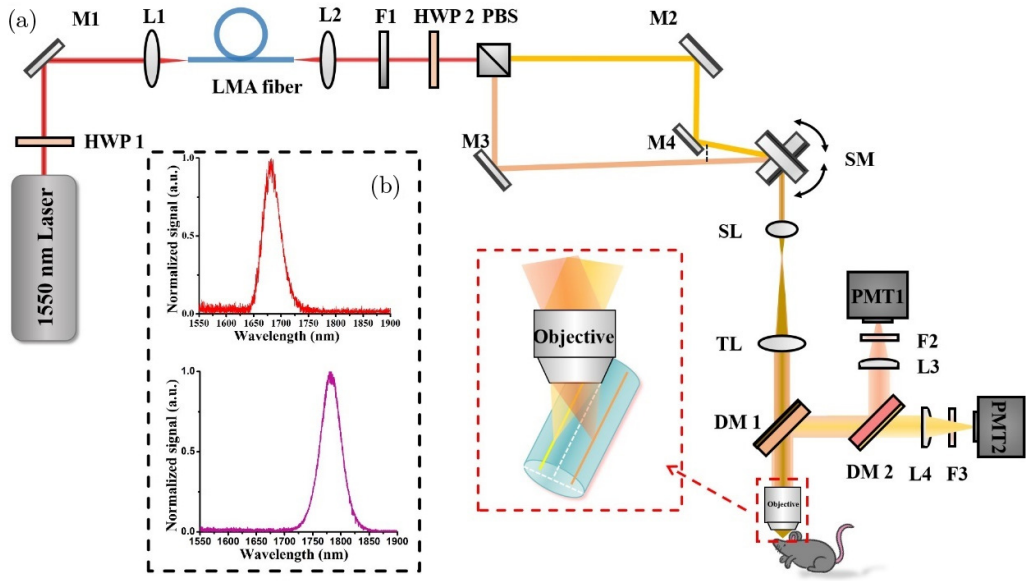

Fig. 1. (a) Experimental setup of dual-wavelength third-harmonic-generation line-scanning imaging system. HWP: Half-wave plate; L1 and L2: Focusing and collimating lens; SL and TL: Scan lens and tube lens; F1: Long-pass filter; F2 and F3: Band-pass filter; M: Mirror; DM: Dichroic mirror; PBS: Polarization beam splitter. Zooming in on the objective section, the red box indicates the schematic of the radial symmetric position of the dual-line scan within the vessel. (b) Measured optical spectra of the 1680 nm (red) and 1780 nm (purple) femtosecond solitons.

widths of the 1680 nm and 1780 nm solitons are 146 fs and 151 fs, respectively. Moreover, the two beams were offset at an angle on the scan mirror of a multiphoton microscope (MOM, Sutter), in order to separate them when focusing on the sample. Through a water-immersion objective lens (XPLN25XSVMP2, Olympus) with D_2O immersion, the optical power on the sample surface was 20 and 22 mW for 1680 and 1780 nm excitations, respectively. The scanning parameters of the system are as follows: The line-scanning speed was 1 ms/line, the pixel size of the two-dimensional image was 512×512 pixels, and the scanning line size of 50 μm. For signal collection, THG signals excited at 1780 nm were detected by a GaAs PMT (H7422-50, Hamamatsu) with a 630/92 bandpass filter (FF01-630/92-25, Semrock). A GaAsP PMT (H7422-40, Hamamatsu) with a 540/80 bandpass filter (FF01-540/80-25, Semrock) was used to collect THG signal from 1680 nm excitation laser. The two channels of THG signals were simultaneously acquired.

2.2. *Animal procedures*

All the mice were from Guangdong Medical Animal Experimental Center, China. The protocols and handling of the animals had been approved by the Animal Ethics Committee of Shenzhen University Medical College.

In mice (C57, female, 7–8 weeks, ~18 g), craniotomy was performed for imaging. Before the experiment, all instruments were sterilized with alcohol, including forceps, scissors, drill and glass coverslips. First, the scalp and periosteum of anesthetized mice were removed with scissors. Second, a home-made head ring was attached to the skull with dental cement. Then, we found suitable target blood vessels with the skull infiltrated with saline. Next, the skull was slowly polished with a drill in a circular motion, centered on target blood vessel, until the skull was about to fall off. Then, the skull was removed with tweezers to create a cranial window about 3 mm in diameter. At this time, the brain was exposed to air and washed with saline. After that, the cranial window was sealed with a cover glass (5 mm diameter) using dental cement. Finally, the mouse was placed in the microscope for *in vivo* imaging. The mouse was kept anesthetized with isoflurane air anesthesia and their body temperature was maintained with a heating pad during the entire experiment.

2.3. *Measurement of blood flow velocity and relative difference analysis*

RBCs can generate third-harmonic signals without labeling. Line scanning is a well-established technique for measuring blood flow velocity. Here, we first moved two scan-lines to radially symmetric positions in the target vessel with the dual-wavelength THG microscopy. The steps are as follows: (1) Move the objective lens so that the equatorial surface of the vessels in one of the channels is in the center of the field of view, and at the same time, the vessels in both channels can be seen to be deviated in radial position. (2) After measuring the distance difference between the radial positions of the two channels, the scan line of the channel moves half the distance of the distance difference, and the other channel moves simultaneously, so that the scan lines of the two channels are in a symmetrical position. (3) After measuring a set of data, adjust the optical path, so that the two scan lines spacing changes, and then repeat the above operation, you can get another set of radial symmetric position of the data and so on to obtain multiple sets of radially symmetric position of the line scan results.

Then, under the simultaneous excitation of two different wavelengths, continuous line-scanning was carried out along a straight line, and two-dimensional time-space images are recorded in two channels. As RBCs flowed in the blood vessels, a series of oblique stripes were acquired in the 2D images. These streaks can be used to measure flow velocity. We used this method to measure blood flow velocity in four groups of radially symmetric positions within a single vessel with 1 KHz scan rate.

Next, we converted the pixel value generated by RBCs movement in the time-space image into microns (Δx) and calculated the velocity using Eq. (1), where Δt is the time between line-scans.[33] We used an established algorithm to calculate the blood flow velocity[34] with our own imaging parameters. From this, we obtained instantaneous velocity versus time at the radially symmetric positions in the target vessel.

$$v = \frac{\Delta x}{\Delta t}. \tag{1}$$

To quantitatively determine the symmetry of the blood flow velocity, we used Eq. (2) to calculate the relative difference (δ), where v_1 and v_2 denote

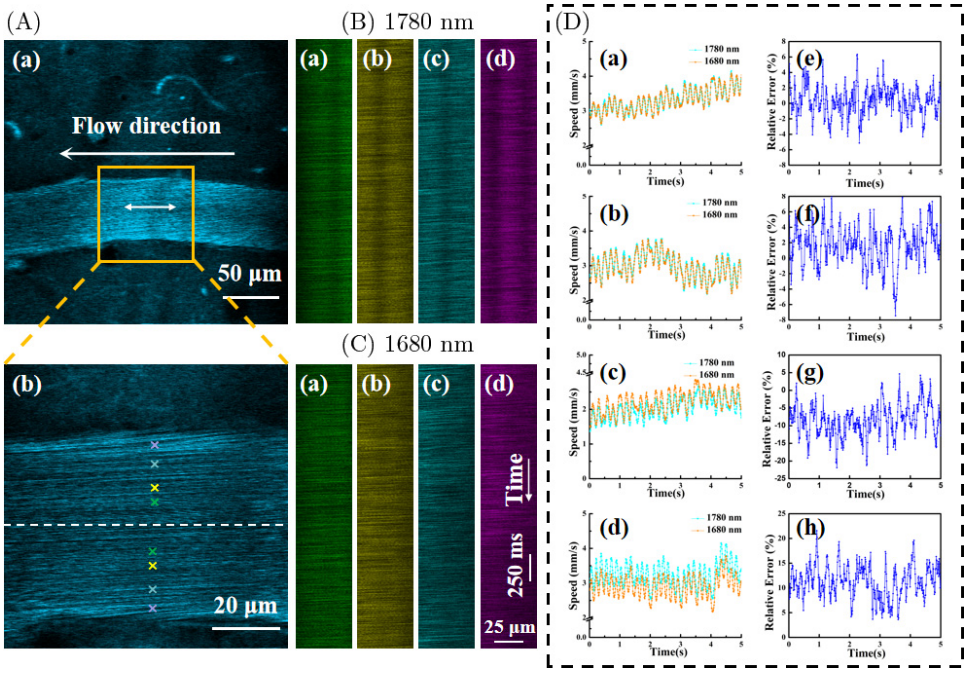

Fig. 2. Line scanning and measured blood flow velocity versus time at the radially symmetric positions in a venule. (A) The 2D image of target venule (a). Scale bar: 50 μm. (b) is the image of the yellow box in (a) magnified three times. Scale bar: 20 μm. (B) and (C) are the line-scan results under 1780 nm and 1680 nm excitation, with the same color indicating the results of a set of radially symmetric line scanning positions in A(b) with "×". Scale bar: 25 μm × 250 ms. (D) Calculated blood flow velocities versus time (a)–(d) and the corresponding relative velocity difference versus time (e)–(h).

the velocity obtained from line-scan at 1780 nm and 1680 nm wavelengths at radially symmetric positions, respectively. Here, we consider a relative difference within ±10% as good symmetry of blood flow velocity, otherwise poor.

$$\delta = \frac{v_1 - v_2}{\frac{v_1+v_2}{2}} \times 100\%. \quad (2)$$

3. Results

Venules and arterioles were first identified by their flow direction and general appearance.[35] Then, we performed dual-wavelength THG imaging and simultaneously measured the instantaneous velocities at two radially symmetric positions in the vessel. Figure 2(A(a)) shows the THG imaging results of a target venule in the brain excited at 1780 nm, and the white arrows indicate the direction of blood flow from right to left. Zooming onto the blood vessel in the yellow box (Fig. 2(A(b))), the white dashed line indicates the center of the equatorial plane of blood vessels, and the "×" marks with the same color on both sides indicate a set of radially symmetrical line scan positions. The upper half of the blood vessel was imaged by 1680 nm, and the corresponding line-scanning results are shown in Fig. 2(C). Likewise, the lower half was imaged by 1780 nm with the line-scanning results shown in Fig. 2(B).

Table 1. Measured mean velocities of the venule and arteriole at different positions.[a]

Type	Wavelength	Position 1 (mm/s)	Position 2 (mm/s)	Position 3 (mm/s)	Position 4 (mm/s)
Venule	1680 nm	3.31	2.95	2.20	2.91
	1780 nm	3.32	3.00	2.03	3.25
Arteriole	1680 nm	−12.94	−8.58	−5.30	−3.08
	1780 nm	−13.12	−9.11	−6.52	−4.09

Notes: [a]Positions 1–4 represent four groups of radially symmetric blood flow velocity measurement positions, with directions from the middle to the walls. Negative sign indicates different direction of blood flow.

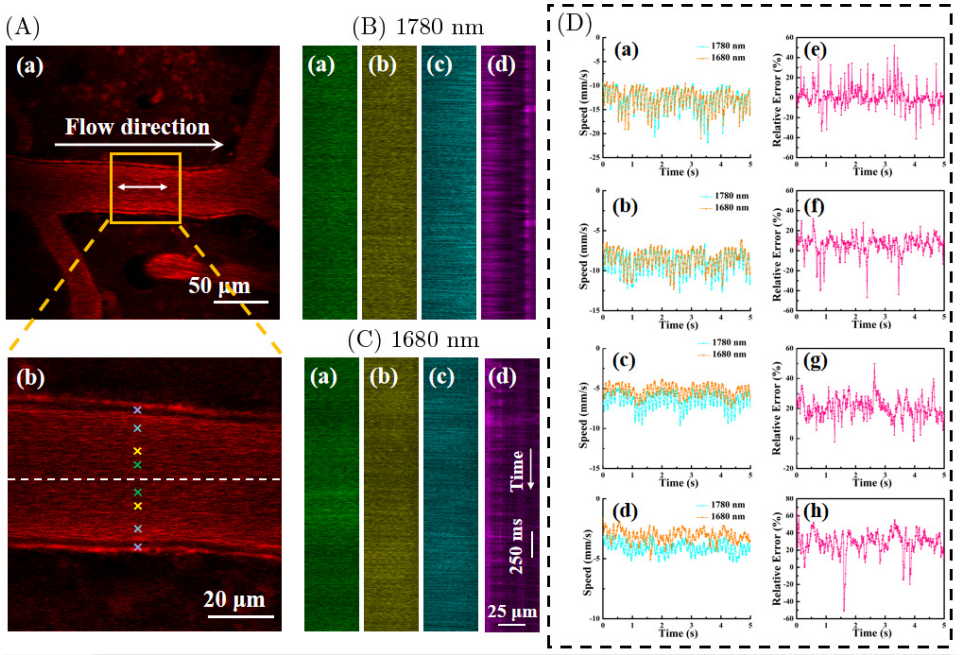

Fig. 3. Line scanning and measured blood flow velocity versus time at the radially symmetric positions in an arteriole. (A) The 2D image of target venule. (a) Scale bar: 50 μm. (b) is the image of the yellow box in (a) magnified three times. Scale bar: 20 μm. (B) and (C) are the line-scan results under 1780 nm and 1680 nm excitation, with the same color indicating the results of a set of radially symmetric line scanning positions in A(b) with "×". Scale bar: 25 μm × 250 ms. (D) Calculated blood flow velocities versus time (a)–(d) and the corresponding relative velocity difference versus time (e)–(h).

The velocities at the symmetrical position of the venules were calculated and statistically analyzed over time, as shown in Fig. 2(D). The velocity and relative difference results at the radial symmetrical position of the venules were obtained in four groups. The four groups of velocity data (Figs. 2(D)(a)–(d)) correspond to the four groups of symmetric positions in Fig. 2(A)(b). The mean velocities of the venule are summarized in Table 1. Furthermore, the relative difference of the first two groups (Figs. 2(D)(a) and 2(b)) is within 10% (Figs. 2(D)(e) and 2(f)), indicating that the flow velocity at the position of venules near the center of blood vessels has good symmetry. The relative difference for the latter two groups (Figs. 2(D)(g) and 2(h)) exceeds 10%, indicating poor symmetry of flow velocity near the vessel wall.

For arteriole with a diameter of 40 μm, the measured results are shown in Fig. 3, with white arrows indicating the direction of blood flow. Compared with the venule in Fig. 2, the blood flow velocities are faster with almost horizontal stripes (Figs. 3(B) and 3(C)). The mean velocities of the arteriole are also summarized in Table 1. In addition to this, it can be seen from Figs. 3(D(e)–(h)) that the symmetry of the arterial blood flow velocity is better near the middle than near the vessel wall, but significantly worse than the radial symmetry of the venule.

4. Discussion

According to Table 1, we can know that the blood flow velocity is fast in the middle of the vessel and decreases gradually in the direction of the vessel wall on both sides. We have done measurements on five blood vessels (two arterioles and three venules) from five different mice (including those in Figs. 2 and 3), all of which show the same trend of velocity symmetry, which are summarized in Table 2. We also performed statistical analysis of the measured mean relative velocity differences for venules. The measured mean $\pm$ standard deviation (SD) values for position 1, 2, 3, and 4 are $2.3 \pm 2.3\%$, $2.9 \pm 2.8\%$, $5.5 \pm 3.0\%$, and $12.5 \pm 5.4\%$, respectively. For this statistical analysis, we took the absolute values of the relative velocity difference, since we were only concerned with their magnitude rather than the sign.

5. Conclusions

Theoretical analysis for blood flow often assumes for simplicity that the flow velocity is radially symmetric. However, this oversimplified assumption may not be valid under practical conditions and needs experimental verification. Previous measurement technologies lack high spatial and temporal resolution. To address these issues, here, we demonstrate a label-free measurement technique based on MPM with a nonlinear optical signal purely from an intrinsic origin (RBCs). Moreover, this technology can be used to measure instantaneous blood flow velocities in a vessel at two radially symmetric positions simultaneously.

Through our measurement, we show that the radial symmetry of blood flow velocity in venules and arterioles is different from the simplified symmetric model. We measured the blood flow speed of arterioles and venules using line scans in mouse brain *in vivo*, and indicated a distribution of rapid flow in the middle and slow flow on both sides. For venules and arteriole, the symmetry of blood flow velocity is good near the middle of the vessel (relative velocity difference $\delta < 10\%$), while the symmetry of blood flow velocity becomes worse and not so symmetric close to the vessel wall ($\delta > 10\%$). Furthermore, the symmetry of arterial flow velocity is poorer than the venule. Our more accurate results may provide guidelines for designing fluidic devices to more accurately mimic blood flow in real blood vessels.

Table 2. The mean relative velocity differences of the venules and arterioles.

Type	Blood vessel #	Position 1	Position 2	Position 3	Position 4
Venule	1	0.3%	1.6%	−8%	11.3%
	2	1.0%	1.1%	−2.1%	−7.8%
	3	−5.7%	−6.1%	−6.3%	−18.4%
Arteriole	1	−1.6%	−4.9%	−23.6%	−52.4%
	2	1.2%	6.0%	20.5%	28.7%

Acknowledgments

This work is funded by the National Natural Science Foundation of China (Grant/Award Numbers 62075135 and 61975126), the Science and Technology Innovation Commission of Shenzhen (Grant/Award Numbers JCYJ20190808174819083 and JCYJ20190808175201640), Shenzhen Science and Technology Planning Project (ZDSYS 20210623092006020).

Conflicts of Interest

The authors declare that there are no conflicts of interest relevant to this paper.

References

1. D. D. Backer, K. Donadello, D. O. Cortes, "Monitoring the microcirculation," *J. Clin. Monit. Comput.* **26**, 361–366 (2012).
2. A. S. Popel, P. C. Johnson, "Microcirculation and hemorheology," *Annu. Rev. Fluid Mech.* **37**, 43–69 (2005).
3. P. Carmeliet, "Angiogenesis in health and disease," *Nat. Med.* **9**, 653–660 (2003).
4. R. H. Adams, K. Alitalo, "Molecular regulation of angiogenesis and lymphangiogenesis," *Nat. Rev. Mol. Cell Biol.* **8**, 464–478 (2007).
5. R. K. Jain, "Molecular regulation of vessel maturation," *Nat. Med.* **9**, 685–693 (2003).
6. E. P. Meyer, A. Ulmann-Schuler, M. Staufenbiel, T. Krucker, "Altered morphology and 3D architecture of brain vasculature in a mouse model for Alzheimer's disease," *PNAS* **105**, 3587–3592 (2008).
7. M. P. Pase, N. A. Grima, C. K. Stough, A. Scholey, A. Pipingas, "Cardiovascular disease risk and cerebral blood flow velocity," *Stroke* **43**, 2803–2805 (2012).
8. A. Cinar, G. Cetin, O. A. Kadirhan, S. Turgut, I. Ekinci, T. Asil, "Determination of cerebral blood flow velocity and microembolic signals in essential thrombocytosis by transcranial doppler ultrasonography," *Neurol. Res.* **43**, 157–163 (2021).
9. D. S. Long, M. L. Smith, A. R. Pries, K. Ley, E. R. Damiano, "Microviscometry reveals reduced blood viscosity and altered shear rate and shear stress profiles in microvessels after hemodilution," *PNAS* **101**, 10060–10065 (2004).
10. G. P. Galdi, A. M. Robertson, R. Rannacher, S. Turek, *Hemodynamical Flows: Modeling, Analysis and Simulation* (Birkhäuser, Boston, 2008).
11. A. Grinvald, E. Lieke, R. D. Frostig, C. D. Gilbert, T. N. Wiesel, "Functional architecture of cortex revealed by optical imaging of intrinsic signals," *Nature* **324**, 361–364 (1986).
12. R. D. Frostig, E. E. Lieke, D. Y. Tso, A. Grinvald, "Cortical functional architecture and local coupling between neuronal activity and the microcirculation revealed by in vivo high-resolution optical imaging of intrinsic signals," *PNAS* **87**, 6082–6086 (1990).
13. A. K. Dunn, "Dynamic imaging of cerebral blood flow using laser speckle," *J. Cereb. Blood Flow Metab.* **21**, 195–201 (2001).
14. H. Li, K. Liu, L. Yao, X. Deng, Z. Zhang, P. Li, "ID-OCTA: OCT angiography based on inverse SNR and decorrelation features," *J. Innov. Opt. Heal. Sci.* **14**, 2130001 (2021).
15. B. M. Ances, J. H. Greenberg, J. A. Detre, "Laser doppler imaging of activation-flow coupling in the rat somatosensory cortex," *Neuroimage* **10**, 716–723 (1999).
16. S. Ogawa, D. W. Tank, R. Menon, J. M. Ellermann, S. G. Kim, H. Merkle, K. Ugurbil, "Intrinsic signal changes accompanying sensory stimulation: Functional brain mapping with magnetic resonance imaging," *PNAS* **89**, 5951–5955 (1992).
17. P. A. Dyachenkotimoshina, A. N. Bashkatov, D. A. Alexandrov, V. I. Kochubey, V. V. Tuchin, "Laser speckle contrast imaging for monitoring of acute-pancreatitis at ischemia-reperfusion injury of the-pancreas in rats," *J. Innov. Opt. Heal. Sci.* **15**, 13 (2022).
18. D. Fukumura, F. Yuan, W. L. Monsky, Y. Chen, R. K. Jain, "Effect of host microenvironment on the microcirculation of human colon adenocarcinoma," *Am. J. Pathol.* **151**, 679–688 (1997).
19. D. M. Brizel, B. Klitzman, J. M. Cook, J. Edwards, M. W. Dewhirst, "A comparison of tumor and normal tissue microvascular hematocrits and red cell fluxes in a rat window chamber model," *Int. J. Radiat. Oncol.* **25**, 269–276 (1993).
20. B. Endrich, H. Reinhold, J. Gross, M. Intaglietta, "Tissue perfusion inhomogeneity during early tumor growth in rats," *J. Natl. Cancer Inst.* **62**, 387–395 (1979).
21. M. L. Smith, D. S. Long, E. R. Damiano, K. Ley, "Near-wall micro-PIV reveals a hydrodynamically relevant endothelial surface layer in venules in vivo," *Biophys. J.* **85**, 637–645 (2003).
22. W. S. Kamoun, S.-S. Chae, D. A. Lacorre, J. A. Tyrrell, M. Mitre, M. A. Gillissen, D. Fukumura, R. K. Jain, L. L. Munn, "Simultaneous measurement of RBC velocity, flux, hematocrit and shear rate in vascular networks," *Nat. Meth.* **7**, 655–660 (2010).
23. I. H. Sarelius, B. R. Duling, "Direct measurement of microvessel hematocrit, red cell flux, velocity, and

transit time," *Am. J. Physiol.* **243**, H1018–1026 (1982).
24. J. J. Bishop, P. R. Nance, A. S. Popel, M. Intaglietta, P. C. Johnson, "Effect of erythrocyte aggregation on velocity profiles in venules," *Am. J. Physiol.* **280**, H222–H236 (2001).
25. W. Denk, J. H. Strickler, W. W. Webb, "Two-photon laser scanning fluorescence microscopy," *Science* **248**, 73–76 (1990).
26. D. Débarre, W. Supatto, A.-M. Pena, A. Fabre, T. Tordjmann, L. Combettes, M.-C. Schanne-Klein, E. Beaurepaire, "Imaging lipid bodies in cells and tissues using third-harmonic generation microscopy," *Nat. Meth.* **3**, 47–53 (2005).
27. M. J. Farrar, F. W. Wise, J. R. Fetcho, C. B. Schaffer, "In vivo imaging of myelin in the vertebrate central nervous system using third harmonic generation microscopy," *Biophys. J.* **100**, 1362–1371 (2011).
28. K. Wang, Y. Pan, X. Chen, S. Tong, H. Liang, Y. Lu, P. Qiu, "3-photon fluorescence and third-harmonic generation imaging of myelin sheaths in mouse digital skin in vivo: A comparative study," *J. Innov. Opt. Health Sci.* **15**, 2250003 (2022).
29. X. Chen, Y. Pan, P. Qiu, K. Wang, "Deep-skin third-harmonic generation (THG) imaging in vivo excited at the 2200 nm window," *J. Innov. Opt. Health Sci.* **Online Ready**, 2243004 (2022), doi: 10.1142/S1793545822430040.
30. H. Liu, Z. Zhuang, S. Tong, W. Xin, J. Li, P. Qiu, K. Wang, X. Chen, "In vivo deep-brain blood flow speed measurement through third-harmonic generation imaging excited at the 1700-nm window," *Biomed. Opt. Exp.* **11**, 2738–2744 (2020).
31. D. Kobat, M. E. Durst, N. Nishimura, A. W. Wong, C. B. Schaffer, C. Xu, "Deep tissue multiphoton microscopy using longer wavelength excitation," *Opt. Exp.* **17**, 13354–13364 (2009).
32. H. Cheng, X. Chen, J. Zhong, J. Li, P. Qiu, K. Wang, "Label-free measurement of wall shear stress in the brain venule and arteriole using dual-wavelength third-harmonic-generation line-scanning imaging," *Opt. Lett.* **47**, 5618–5621 (2022).
33. S. Dietzel, J. Pircher, A. K. Nekolla, M. Gull, A. W. Brändli, U. Pohl, M. Rehberg, "Label-free determination of hemodynamic parameters in the microcirculaton with third harmonic generation microscopy," *PLoS One* **9**, e99615 (2014).
34. T. N. Kim, P. W. Goodwill, Y. Chen, S. M. Conolly, C. B. Schaffer, D. Liepmann, R. A. Wang, "Line-scanning particle image velocimetry: An optical approach for quantifying a wide range of blood flow speeds in live animals," *PloS One* **7**, e38590 (2012).
35. A. Y. Shih, J. D. Driscoll, P. J. Drew, N. Nishimura, C. B. Schaffer, D. Kleinfeld, "Two-photon microscopy as a tool to study blood flow and neurovascular coupling in the rodent brain," *J. Cerebr. Blood Flow Metab.* **32**, 1277–1309 (2012).